NANO LETTERS

pubs.acs.org/NanoLett Letter

Charging and Charged Species in Quantum Dot Light-Emitting Diodes

Logan P. Keating, Hyunho Lee, Steven P. Rogers, Conan Huang, and Moonsub Shim*

Cite This: *Nano Lett.* 2022, 22, 9500−9506 Read Online

ACCESS | Metrics & More | Article Recommendations | Supporting Information

ABSTRACT: Despite recent rapid advances in improving quantum dot light-emitting diodes, many fundamental aspects of the device operating mechanism remain unresolved. Through transient electroluminescence and time-resolved photoluminescence measurements, the effects of offset voltage on charging and charge transport are examined. First, capacitive charging occurs with a time constant of ∼500 ns, followed by electron transport through quantum dots with a mobility of $\sim 10^{-5}$ cm^2 V^{-1} s^{-1}. Hole injection then initiates an electroluminescence rise that is independent of offset voltage. The photoluminescence lifetime is also unaffected by the offset voltage, indicating no injection of charges into the quantum dots or on their surfaces prior to the voltage pulse. A slower equilibration to steady-state electroluminescence is dependent on the offset voltage, indicative of another charging process. Elemental mapping shows that ZnO deposition from solution can lead to the diffusion of charged species into the quantum dot layer, which may cause the slower process.

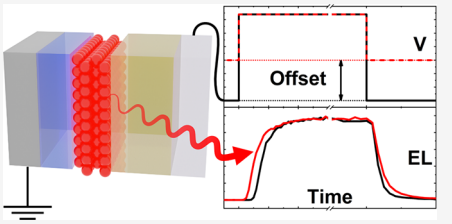

KEYWORDS: *quantum dot LED, colloidal semiconductor nanocrystals, transient electroluminescence, offset voltage*

Colloidal quantum dots (QDs) are candidates for transformative advances in many areas, including photovoltaics,[1] bioimaging,[2] optoelectronics,[3] flexible electronics,[4,5] and high-brightness displays.[6,7] Many desirable properties such as tunable emission wavelength[8,9] with high efficiency,[10,11] brightness,[12] and color purity[13] make QDs ideal as luminescent down-converters and electrically driven light sources. Despite these advantages and the experimental demonstration of QD light-emitting diodes (QD-LEDs) nearly 3 decades ago,[14,15] many challenges, such as efficiency droop, short device lifetimes, and device-to-device variation, remain. Key phenomena that contribute to these challenges include thermal-[16] and electric-field-dependent[17,18] quenching, Auger recombination,[19−23] and organic hole transport layer (HTL) degradation.[24−28]

Transient electroluminescence (TrEL), which has been studied and utilized extensively in organic LEDs,[29−32] is well-suited to address some of these critical issues within real working QD-LEDs. For CdSe-based QD-LEDs, in addition to measuring how fast these devices can turn on and off,[7] TrEL has been used to investigate energy transfer,[33] doping electron transport layers (ETL),[34] and charge trapping by surface ligands.[35] The effects of different HTLs[36] and insulating layers[37] in $CuInS_2$/ZnS QD-LEDs and excess holes in InP QD-LEDs have also been examined via TrEL.[38,39] Yet, many fundamental aspects of device operation such as time constants for charge accumulation at the QD/charge transport layer (CTL) interface and electron mobility in core/shell QD solids remain unexamined.

Here, the transient response of CdSe/ZnSe/ZnS core/shell QD-LEDs is explored through TrEL measurements. The dependence of the EL onset delay on the offset and driving voltages is analyzed by a simple RC circuit and electron drift model to provide capacitive charging time constant and electron mobility. Offset-voltage-dependent slow equilibration during the driving voltage pulse is also observed. The potential origin of the slow equilibration is discussed with respect to Zn- and O-containing species diffusing into the QD emitting layer (EML) during solution spin-casting of the ZnO ETL.

The QD-LEDs examined in this work consist of a prepatterned ITO substrate, a PEDOT:PSS hole injection layer, a TFB HTL, a CdSe/ZnSe/ZnS core/shell/shell QD EML, a ZnO ETL, and an Al cathode. All layers above the ITO substrate are spin-cast from solution, with the exception of the Al electrodes, which are deposited by thermal evaporation. The details of the QD synthesis and device fabrication procedure are available in the Supporting Information. Characterization including TEM, UV−vis absorption, photoluminescence (PL) spectra of the QDs used, and a device cross-sectional TEM image are available in Figures S1 and S2. The expected band alignment of the QD-LED and the device schematic are shown in the insets of Figures 1a and 1b, respectively. Typical static EL spectra at different driving voltages are shown in Figure 1a. The devices examined here have a peak external quantum

Received: September 13, 2022
Revised: November 29, 2022
Published: December 2, 2022

https://doi.org/10.1021/acs.nanolett.2c03564
Nano Lett. 2022, 22, 9500−9506

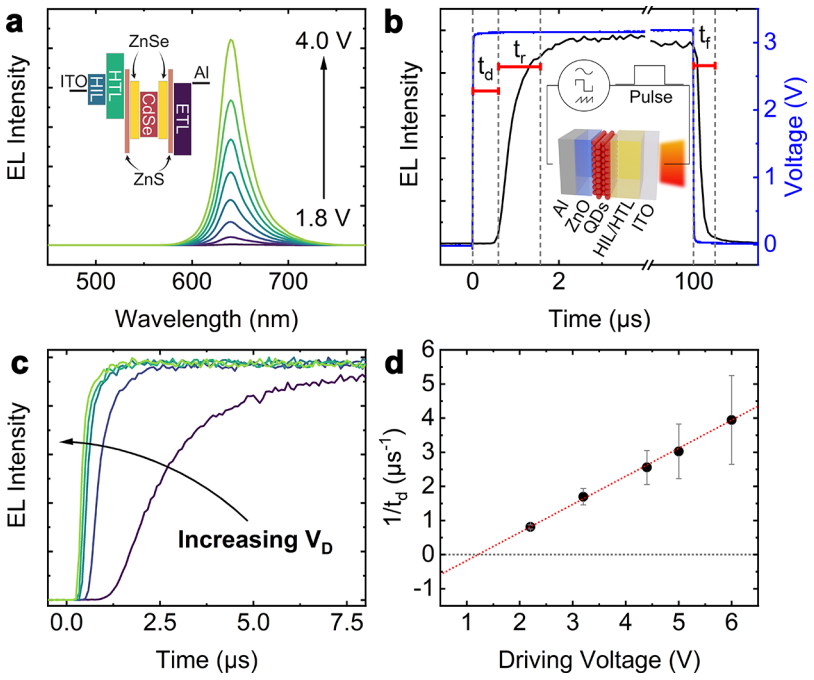

Figure 1. (a) Static electroluminescence spectra at different driving voltages and the device band diagram (inset). (b) Temporal profile of a driving voltage pulse (blue line, shown for V_D = 3.2 V) and the corresponding EL response (black line) for TrEL measurements for a QD-LED. The inset is the schematic of the device structure under a voltage pulse. After the start of the voltage pulse, there is a short delay to the onset of EL which then rises to a steady state intensity. The EL fall is seen when the bias is removed at 100 μs. The delay time (t_d), rise time (t_r), and fall time (t_f) are illustrated in the plot. (c) TrEL rise region for a device, with the increasing driving voltage leading to shorter delay to onset of EL and a more rapid rise. (d) Inverse delay time plotted as a function of increasing driving voltage. The expected linear relationship is obtained as shown by the linear regression analysis with an adjusted R^2 value of 0.997.

efficiency (EQE) of ~7−9% at low operating voltages with >1000 cd m^{-2} luminance at peak EQE (Figures S3 and S4). The maximum luminance is >10000 cd m^{-2} at higher driving voltages.

TrEL measurements are performed by applying a square voltage pulse at a 2.94 kHz repetition rate while synchronously measuring the light emitted from the LED. The voltage pulse (blue), with its maximum referred to here as the driving voltage (V_D), and the resulting EL signal (black) are shown in Figure 1b. The measurement setup is schematically shown in Figure S5, and the experimental details are described in the Supporting Information. After the voltage pulse is applied, there is a delay in the onset of the EL signal because carrier injection and transport must occur prior to exciton formation and radiative recombination. This delay time (t_d) is indicated in Figure 1b along with the rise time (t_r) and the fall time (t_f). The delay time is typically defined as the x-intercept of the "linear" region of the TrEL rise sigmoid.[29,40] Because the "linear" region of the sigmoid is not rigorously defined, we have automated a similar procedure to reduce human error (Figure S6).

Figure 1c shows the EL rise region for different V_D, where both t_d and t_r decrease with increasing V_D. Rigorous modeling of TrEL requires consideration of many complicating factors and progress is being made by modifying the Langevin model employed in OLEDs,[29,41] but many of the necessary parameters are not known and simulations become difficult with increasing number of QD layers.[42,43] For a simple and intuitive understanding of V_D dependence of t_d, we consider the following. Assuming a linear potential drop across the device, t_d can be estimated from the drift velocity equation ($\vec{v} = \mu\vec{E}$):[44−47]

$$t_d = \frac{d^2}{\mu \cdot V_D} \quad (1)$$

where d is the distance carriers traverse and μ is the carrier mobility.

In general, eq 1 is complicated by the multiple layers that carriers must traverse and the need to consider different mobilities for electrons and the holes. However, we can make some simplifying assumptions. First, given that the electron mobility (μ_e) in ZnO ETL[48] and the hole mobility (μ_h) in TFB HTL[49] should be orders of magnitude higher than those in QD EML,[50,51] we assume that the limiting factor in t_d is the charge transport through the thickness of the QD layer or $d \approx d_{QD}$. We also assume that the majority of the potential drop is across the QD EML. Furthermore, the lower barrier for electron injection (Figure 1a) than hole injection and, more importantly, μ_e being much higher than μ_h for CdSe QDs[50,51] allow the approximation $\mu \approx \mu_e$. With these simplifications, the inverse delay time (t_d^{-1}) scales linearly with V_D.

Figure 1d shows t_d^{-1} plotted as a function of V_D, where the expected linear relationship is obtained. Using the nominal QD EML thickness of 40 nm, $\mu_e \approx 1.3 \times 10^{-5}$ cm^2 V^{-1} s^{-1} is obtained as a fitting parameter. The nonzero x-intercept of 1.17 V may be accounted for by considering the "built-in" voltage (V_{bi}) of the device. V_{bi} may be expected to be the difference in work functions of TFB[52] and ZnO[53,54] (~1 eV). However, the doping states of TFB and ZnO are not known exactly, and work functions can vary significantly with different surface adsorption.

Applying a DC offset voltage (V_{offset}) prior to the driving voltage pulse should cancel out V_{bi} and provide additional

https://doi.org/10.1021/acs.nanolett.2c03564
Nano Lett. 2022, 22, 9500−9506

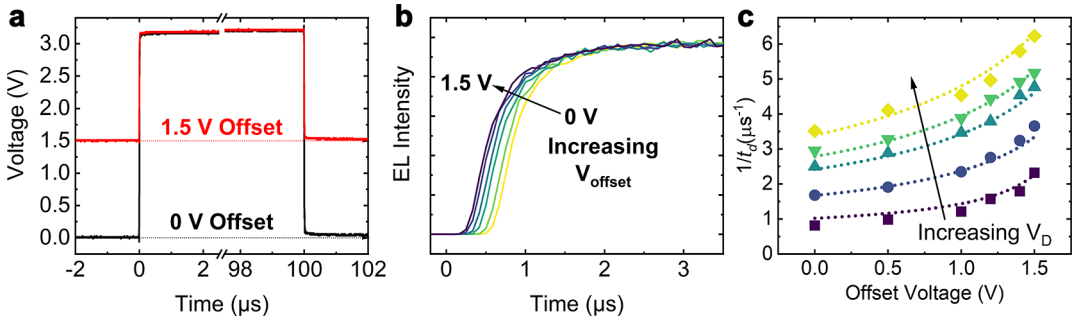

Figure 2. (a) Example of a waveform with a 1.5 V offset voltage and a 3.2 V driving voltage (red line) compared to one without the offset at the same driving voltage (black line). (b) Rise region of the TrEL trace for V_D = 3.2 V and varying offset voltage. (c) Plot of the inverse delay time as a function of the offset voltage for various driving voltages. The results of performing a global fit using eq 4 (dotted lines) show excellent agreement with the experimental data with adjusted R^2 across the data set of 0.987. The fitting parameters are $\mu = 1.7 \times 10^{-5}$ cm^2 V^{-1} s^{-1}, $\tau = 4.7 \times 10^{-5}$ s, and V_{inj} = 1.52 V.

insight. Examples of the measured voltage pulse profile with and without offset are shown in Figure 2a. The rise region of TrEL corresponding to voltage pulses with V_{offset} ranging from 0 to 1.5 V is shown in Figure 2b. The offset voltage dependence was measured from 0 to 1.5 V where the upper limit of 1.5 V was chosen to stay below the turn-on voltage. Figure 2c shows t_d^{-1} extracted from these plots as a function of V_{offset}. While V_{offset} simply canceling out V_{bi} should lead to linear behavior, near-exponential dependence on V_{offset} is observed.

To explain this behavior, we consider a simple RC circuit model, where the QD EML is the dielectric of the capacitor and the CTLs give rise to the series resistance. Then, the time dependence of the voltage drop across the capacitor is given by

$$V(t) = V_D(1 - e^{-t/\tau}) \tag{2}$$

where τ is the RC time constant. As the voltage ramps to V_D, electrons will begin to be injected into the QD EML at some critical voltage, which we will refer to as V_{inj}. Then, t_{inj}, the time to reach V_{inj}, is given by rearranging eq 2 and substituting in t_{inj} and V_{inj} for t and V, respectively:

$$t_{inj} = \tau \ln\left(\frac{V_D}{V_D - V_{inj}}\right) \tag{3}$$

The effect of the offset in the voltage pulse profile is to reduce t_{inj} because we are starting from some fixed V_{offset} rather than 0 V. This reduction in time to t_{inj} can be defined in the same manner as t_{inj} was in eq 3. Because t_d is the sum of the capacitive charging time plus the time for the electrons to transport across the QD EML, we add the capacitive charging time to eq 1, leading to

$$t_d = \frac{d^2}{\mu V_D} + \tau\left(\ln\frac{V_D - V_{offset}}{V_D - V_{inj}}\right) \tag{4}$$

which provides both the V_D and V_{offset} dependence of t_d.

The dotted lines in Figure 2c are the result of global fitting using eq 4. The same data plotted versus V_D are shown in Figure S7. This remarkable agreement with the simple RC circuit model further validates our simplification that the transport through QD EML dominated by electrons is the limiting factor in the delay time for the onset of EL. It also indicates that charge accumulation at the interface between CTLs and the QD EML occurs with an RC time constant of ~500 ns. The injection of electrons into the QD EML initiates at V_{inj} = 1.52 V, which is slightly smaller than the driving voltage at which observable EL occurs. The obtained electron mobility of 1.7×10^{-5} cm^2 V^{-1} s^{-1} is well within the range reported for CdSe QDs.[50,51,55] While the QDs studied here are core/shell QDs whereas most mobilities are reported for core-only QDs, the similar mobility value may suggest that the insulating organic ligand rather than the inorganic shell is the limiting factor. In fact, higher electron mobility has been reported in CdSe QDs with different ligand treatment.[51,56,57]

While t_d is strongly dependent on V_{offset} due to capacitive charging, we note that t_r is independent of V_{offset} (Figure 2b). This behavior is clearly seen when the EL rise region data are collapsed together by setting t_d to be the same (Figure S8). Because t_r is associated with the spread of the emission zone after the injection of holes, which occurs after the initial capacitive charging and electron transport across the QD EML, this behavior can be expected. In the EL fall region, t_f is affected by V_{offset} and exhibits a biexponential behavior (Figure S9), presumably due to exciton recombination and charge extraction to CTLs, both of which, especially the latter, are expected to be V_{offset} dependent. Conversely, the EL rise exhibits single-exponential behavior (Figure S10a). The single-exponential decay fit and the corresponding time constant vs V_D are shown in Figure S10b. Previous reports in both OLED[29] and QD-LED[58] literature have indicated that the rise region can be fitted to a biexponential function, where the fast component is typically assigned to the majority carrier and the slow component to the minority carrier. We initially performed a biexponential fit, but examination of the time constants and amplitudes suggested it was overfitting the data.

Although the single-exponential fit exhibits excellent agreement, there is a complication that arises from a slow equilibration process after the maximum EL intensity is reached. In most devices we have examined, the slow equilibration leads to a small decrease (<7%) in EL from the maximum intensity near the rise region to just before the driving voltage is turned off (Figure 1b). In extreme cases, there is an apparent overshoot in the EL near the rise region. Figure 3 shows an example where the overshoot is significant at negative V_{offset} but disappears at positive V_{offset} slightly below the LED turn-on voltage. In all cases we have examined, there is a slow equilibration in EL, which is accompanied by the corresponding slow decrease in the current density, during the duration of the driving voltage pulse (a more typical example given in Figure S11). While the magnitude of the slow decrease in EL and current varies, it systematically becomes more

https://doi.org/10.1021/acs.nanolett.2c03564
Nano Lett. 2022, 22, 9500−9506

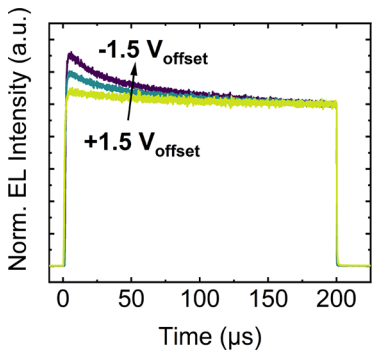

Figure 3. Normalized TrEL traces for V_{offset} = {−1.5, 0, +1.5 V} showing the full equilibrium region. There is a decay over time from a maximum value for the negative offset voltage, while the positive voltage is relatively flat. Note that V_D pulse here is longer (200 μs), and the V_{offset} range has been expanded to negative voltages which appear to amplify the overshoot.

noticeable with more negative V_{offset}, suggesting a possible charging process.

We then consider where the charging might occur. There have been reports of EL overshoot during TrEL measurements. Notably, a varying EL spike upon voltage pulse turnoff has been reported with amine-capped QDs,[59] and a varying degree of overshoot near the EL rise region has been observed with different ETL materials.[34,43] The EL spike near the fall region has been attributed to charge trapping on the surface of the QDs by amine ligands. These charges on the QD surface accumulate during the driving voltage pulse and are released upon removal of the voltage, leading to additional carriers for radiative recombination. Varying the post-turnoff offset bias has indicated that forward bias causes buildup of these charges while negative offset bias after the initial driving voltage pulse helps to release them. A similar EL overshoot upon voltage turnoff has been reported previously in OLEDs.[60−62] However, our observed behavior is the opposite. That is, if our observed overshoot were due to similar surface trapped charges, the overshoot being near the rise rather than the fall region would suggest that the negative offset voltage would enhance the buildup, and the forward driving voltage would cause the release of these charges. Furthermore, based on bias-dependent time-resolved PL (TRPL) discussed later, surface charging is unlikely occurring during the offset voltage.

In the case of ETL composition affecting EL overshoot near the rise region, Kim et al. have attributed this effect to the buildup of electrons at the ETL/QD EML interface.[34] On the other hand, Yu et al. reported a larger EL overshoot with TiO_2 compared to ZnO as ETL.[43] They attributed the larger overshoot to less efficient electron injection with TiO_2 which can lead to larger hole population in the QD film, allowing Auger recombination via positive trions to be more feasible and therefore more nonradiative overall. If the application of negative offset voltage introduces holes into the QD film and causes the overshoot, an initial reduction in EL can be expected. However, the initial TrEL intensity is higher when there is a smaller or more negative offset in our case. Furthermore, the introduction of holes (or electrons) is expected to lead to shorter PL lifetime due to fast Auger recombination. Figure 4a,b shows the results of TRPL measurements on a QD-LED under bias. In the voltage range examined, which is the same as our TrEL offset voltage range, there is no measurable EL, and the PL lifetime remains constant. A change in PL lifetime with applied bias has been observed when there are pre-existing electrons (e.g., due to electron transfer from ETL) and the applied bias changes that population[19] or when the incident laser excitation for TRPL causes photocurrent.[7] The lack of PL lifetime change within the ±1.5 V bias range indicates that charge carriers are not injected with the application of the offset voltage (Figure 4b).

Charges trapped at the surface of QDs would also affect the PL lifetime because they will affect nonradiative recombination pathways. Decreasing PL efficiency has been observed in CdSe/CdS core/shell QD-LEDs when increasing forward bias causes the reduction of surface Cd carboxylates at ∼1 V and higher.[63] In our QD-LEDs the PL lifetime remains independent of bias (Figure 4b). Hence, if offset voltage induced charging is occurring, it must be occurring elsewhere in the QD-LED. The plausible locations of charge accumulation during the DC offset voltage that causes EL overshoot are the CTL/EML interface or within the QD matrix. To this end, we have performed cross-sectional STEM imaging and EDX elemental mapping of pseudodevices to consider the effect of spin-casting ZnO ETL from solution (Figure 5). The top set of images (Figures 5a−d) correspond to the control case where QDs were spin-cast onto predeposited ZnO. The bottom images (Figures 5e−h) correspond to our conventional device structure where ZnO was spin-cast on top of QDs. Note that we have used CdSe QDs without an inorganic shell because the ZnSe/ZnS shell would lead to Zn signal that may not be distinguishable from that of ZnO. STEM-EDX maps of the QDs-on-top case exhibit a clear distinction between where Zn and the majority of O are present and where Cd is present. However, in our device-equivalent case, there is significant penetration of Zn signal into the QD region. The interface between the CdSe QD region and the ZnO region cannot be

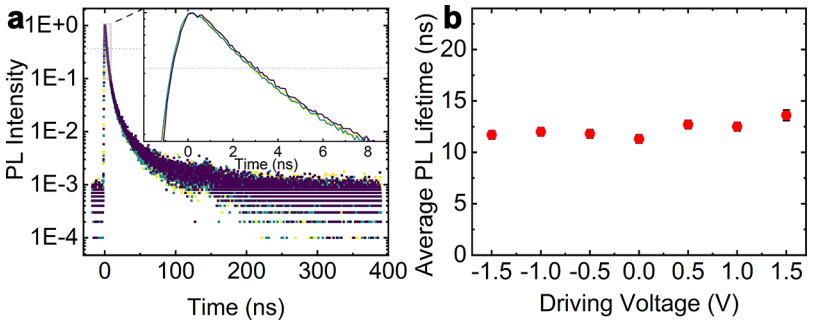

Figure 4. (a) Time-resolved photoluminescence of QD-LED under −1.5, 0, and 1.5 V bias where there is no contribution from EL. The inset shows early time region. (b) Average PL lifetime as a function of applied voltage. No significant change in the average PL lifetime is observed.

https://doi.org/10.1021/acs.nanolett.2c03564
Nano Lett. 2022, 22, 9500−9506

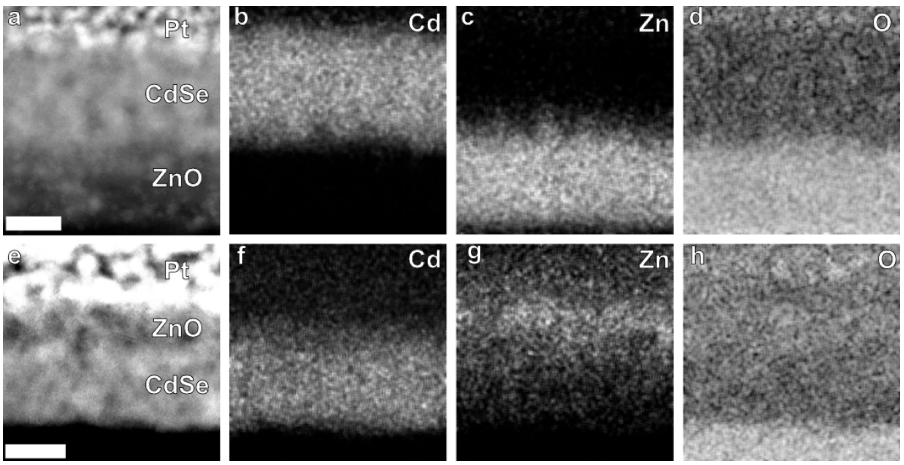

Figure 5. (a) Cross-sectional high-angle annular dark field (HAADF) micrograph of a control pseudodevice where CdSe QDs were deposited on top of a ZnO layer. (b–d) Corresponding atomic percent STEM-EDX maps of Cd, Zn, and O. (e) Cross-sectional HAADF micrograph of a pseudo device where ZnO is spin-cast on CdSe QDs, analogous to the device structure examined in this work. (f–h) Corresponding atomic percent STEM-EDX maps of Cd, Zn, and O. The Zn map indicates penetration of the Zn-containing species into the CdSe QD layer. The O map shows very little partitioning between layers. Scale bars shown in (a) and (e) are 10 nm, and the scale is the same across all images. The Pt protecting layer deposited as a part of the focused ion beam cross-sectioning process and the SiO_2 substrate are visible at the top and bottom of each micrograph, respectively.

discerned through the O map. That is, when ZnO is spin-cast from solution onto a film of QDs, Zn- and O-containing species can contaminate the QD layer. These species may originate from dissociation of surface Zn and O from ZnO nanoparticles or leftover byproducts of the reaction to synthesize ZnO. We note that the intermixing of ZnO nanoparticles with QDs is not likely given that such an intermixing will likely lead to high local intensities of the Zn signal in the QD layer and the Cd signal in the ZnO layer rather than the uniformly spreading intensity seen in Figure 5g. Furthermore, the bright-field TEM image of a device (Figure S2) shows a distinct interface between ZnO and QDs with no obvious signs of intermixing. Nevertheless, we cannot completely rule out the possibility of very small ZnO particles penetrating the QD layer.

The Zn/O species that diffuse into the QD layer can contribute to the charging process that leads to the overshoot observed in TrEL. The slow equilibration after the overshoot may also be explained by the slow diffusion of such species within the QD matrix under bias. Device-to-device variations in the degree of overshoot may be related to the concentration of these species which is likely to vary due to several factors, including the degree of completion of the ZnO reaction, the age of the ZnO solution, and precipitation/purification. While further studies are needed to characterize what processes such species might undergo with external potential (e.g., electrochemical oxidation/reduction vs charge diffusion) and how that process contributes to varying TrEL response of QD-LEDs, the presence of Zn/O species diffusing from ZnO spin-coating solution into the QD EML can have important consequences in both the device operation and degradation mechanisms. These species likely contribute to the varying overshoot and slow equilibration of EL. They may also facilitate device degradation by promoting oxidation of organics, either the HTL or ligands on QDs. Inverted device structures can mitigate these effects but HTL often needs to be vacuum deposited.[64] Inserting a thin PMMA layer between QDs and ZnO is another potential approach but leads to an insulating layer that degrades electrical characteristics.[65]

In summary, we have examined the effects of an offset voltage on the TrEL characteristics of CdSe/ZnSe/ZnS QD-LEDs. The time constant for capacitive charging, the electron mobility in the QD film, and V_D and V_{offset} dependence of t_d have been obtained through a simple consideration of an RC circuit with electron drift through QDs. Slow equilibration to steady-state EL that varies with V_{offset} has been observed and may be associated with either a charging or charge diffusion process within the QD-LED. The lack of change in PL lifetime under offset bias indicates charged species are unlikely to be carriers in QDs or surface trapped charges. Zn and O species in QD film observed through STEM-EDX may be diffusing in from ZnO spin-casting solution, and these charged species may contribute to the slow equilibration in TrEL and to device-to-device variations. These insights can help to better understand QD-LED operation and device failure mechanisms and to improve the performance of cost-effective, solution-processed devices.

■ ASSOCIATED CONTENT

Supporting Information

The Supporting Information is available free of charge at https://pubs.acs.org/doi/10.1021/acs.nanolett.2c03564.

Synthesis and chemicals, device fabrication, data analysis description, additional figures and analysis (PDF)

■ AUTHOR INFORMATION

Corresponding Author

Moonsub Shim − *Department of Materials Science and Engineering, University of Illinois Urbana−Champaign, Urbana, Illinois 61801, United States;* orcid.org/0000-0001-7781-1029; Email: mshim@illinois.edu

Authors

Logan P. Keating − *Department of Materials Science and Engineering, University of Illinois Urbana−Champaign, Urbana, Illinois 61801, United States;* orcid.org/0000-0002-1106-9658

https://doi.org/10.1021/acs.nanolett.2c03564
Nano Lett. 2022, 22, 9500−9506

Hyunho Lee − *Department of Materials Science and Engineering, University of Illinois Urbana−Champaign, Urbana, Illinois 61801, United States*

Steven P. Rogers − *Department of Materials Science and Engineering, University of Illinois Urbana−Champaign, Urbana, Illinois 61801, United States;* orcid.org/0000-0003-1554-4142

Conan Huang − *Department of Materials Science and Engineering, University of Illinois Urbana−Champaign, Urbana, Illinois 61801, United States*

Complete contact information is available at: https://pubs.acs.org/10.1021/acs.nanolett.2c03564

Funding

Financial support from the U.S. National Science Foundation (Grant No. 2132538) is gratefully acknowledged.

Notes

The authors declare no competing financial interest.

REFERENCES

(1) Kirmani, A. R.; Luther, J. M.; Abolhasani, M.; Amassian, A. Colloidal quantum dot photovoltaics: Current progress and path to gigawatt scale enabled by smart manufacturing. *ACS Energy Lett.* **2020**, *5*, 3069−3100.

(2) Martynenko, I. V.; Litvin, A. P.; Purcell-Milton, F.; Baranov, A. V.; Fedorov, A. V.; Gun'Ko, Y. K. Application of semiconductor quantum dots in bioimaging and biosensing. *J. Mater. Chem. B* **2017**, *5*, 6701−6727.

(3) Kagan, C. R.; Lifshitz, E.; Sargent, E. H.; Talapin, D. V. Building devices from colloidal quantum dots. *Science* **2016**, *353*, aac5523.

(4) Choi, M. K.; Yang, J.; Hyeon, T.; Kim, D. H. Flexible quantum dot light-emitting diodes for next-generation displays. *npj Flexible Electron* **2018**, *2*, 1−14.

(5) Hu, L.; et al. Flexible and efficient perovskite quantum dot solar cells via hybrid interfacial architecture. *Nat. Commun.* **2021**, *12*, 1−9.

(6) Li, X.; Lin, Q.; Song, J.; Shen, H.; Zhang, H.; Li, L. S.; Li, X.; Du, Z. Quantum-Dot Light-Emitting Diodes for Outdoor Displays with High Stability at High Brightness. *Adv. Opt. Mater.* **2020**, *8*, 1901145.

(7) Oh, N.; et al. Double-heterojunction nanorod light-responsive LEDs for display applications. *Science* **2017**, *355*, 616−619.

(8) Brus, L. E. Electron-electron and electron-hole interactions in small semiconductor crystallites: The size dependence of the lowest excited electronic state. *J. Chem. Phys.* **1984**, *80*, 4403−4409.

(9) Rossetti, R.; Nakahara, S.; Brus, L. E. Quantum size effects in the redox potentials, resonance Raman spectra, and electronic spectra of CdS crystallites in aqueous solution. *J. Chem. Phys.* **1983**, *79*, 1086−1088.

(10) Won, Y.-H.; Cho, O.; Kim, T.; Chung, D.-Y.; Kim, T.; Chung, H.; Jang, H.; Lee, J.; Kim, D.; Jang, E. Highly efficient and stable InP/ZnSe/ZnS quantum dot light-emitting diodes. *Nature* **2019**, *575*, 634−638.

(11) Hanifi, D. A.; Bronstein, N. D.; Koscher, B. A.; Nett, Z.; Swabeck, J. K.; Takano, K.; Schwartzberg, A. M.; Maserati, L.; Vandewal, K.; van de Burgt, Y.; Salleo, A.; Alivisatos, A. P. Redefining near-unity luminescence in quantum dots with photothermal threshold quantum yield. *Science* **2019**, *363*, 1199−1202.

(12) Shen, H.; Gao, Q.; Zhang, Y.; Lin, Y.; Lin, Q.; Li, Z.; Chen, L.; Zeng, Z.; Li, X.; Jia, Y.; Wang, S.; Du, Z.; Li, L. S.; Zhang, Z. Visible quantum dot light-emitting diodes with simultaneous high brightness and efficiency. *Nat. Photonics* **2019**, *13*, 192−197.

(13) Huang, L.; Ye, Z.; Yang, L.; Li, J.; Qin, H.; Peng, X. Synthesis of Colloidal Quantum Dots with an Ultranarrow Photoluminescence Peak. *Chem. Mater.* **2021**, *33*, 1799−1810.

(14) Colvin, V. L.; Schlamp, M. C.; Alivisatos, A. P. Light-emitting diodes made from cadmium selenide nanocrystals and a semiconducting polymer. *Nature* **1994**, *370*, 354−357.

(15) Dabbousi, B. O.; Bawendi, M. G.; Onitsuka, O.; Rubner, M. F. Electroluminescence from CdSe quantum-dot/polymer composites. *Appl. Phys. Lett.* **1995**, *66*, 1316−1318.

(16) Sun, Y.; Su, Q.; Zhang, H.; Wang, F.; Zhang, S.; Chen, S. Investigation on Thermally Induced Efficiency Roll-Off: Toward Efficient and Ultrabright Quantum-Dot Light-Emitting Diodes. *ACS Nano* **2019**, *13*, 11433−11442.

(17) Bozyigit, D.; Yarema, O.; Wood, V. Origins of Low Quantum Efficiencies in Quantum Dot LEDs. *Adv. Funct. Mater.* **2013**, *23*, 3024−3029.

(18) Empedocles, S. A.; Bawendi, M. G. Quantum-Confined Stark Effect in Single CdSe Nanocrystallite Quantum Dots. *Science* **1997**, *278*, 2114−2117.

(19) Bae, W. K.; Park, Y.-S.; Lim, J.; Lee, D.; Padilha, L. A.; McDaniel, H.; Robel, I.; Lee, C.; Pietryga, J. M.; Klimov, V. I. Controlling the influence of Auger recombination on the performance of quantum-dot light-emitting diodes. *Nat. Commun.* **2013**, *4*, 2661.

(20) Cragg, G. E.; Efros, A. L. Suppression of Auger Processes in Confined Structures. *Nano Lett.* **2010**, *10*, 313−317.

(21) Vaxenburg, R.; Rodina, A.; Shabaev, A.; Lifshitz, E.; Efros, A. L. Nonradiative Auger Recombination in Semiconductor Nanocrystals. *Nano Lett.* **2015**, *15*, 2092−2098.

(22) Jain, A.; Voznyy, O.; Hoogland, S.; Korkusinski, M.; Hawrylak, P.; Sargent, E. H. Atomistic Design of CdSe/CdS Core−Shell Quantum Dots with Suppressed Auger Recombination. *Nano Lett.* **2016**, *16*, 6491−6496.

(23) García-Santamaría, F.; Chen, Y.; Vela, J.; Schaller, R. D.; Hollingsworth, J. A.; Klimov, V. I. Suppressed Auger Recombination in "Giant" Nanocrystals Boosts Optical Gain Performance. *Nano Lett.* **2009**, *9*, 3482−3488.

(24) Davidson-Hall, T.; Aziz, H. The role of excitons within the hole transporting layer in quantum dot light emitting device degradation. *Nanoscale* **2019**, *11*, 8310−8318.

(25) Chang, J. H.; Park, P.; Jung, H.; Jeong, B. G.; Hahm, D.; Nagamine, G.; Ko, J.; Cho, J.; Padilha, L. A.; Lee, D. C.; Lee, C.; Char, K.; Bae, W. K. Unraveling the Origin of Operational Instability of Quantum Dot Based Light-Emitting Diodes. *ACS Nano* **2018**, *12*, 10231−10239.

(26) Xue, X.; Dong, J.; Wang, S.; Zhang, H.; Zhang, H.; Zhao, J.; Ji, W. Degradation of quantum dot light emitting diodes, the case under a low driving level. *J. Mater. Chem. C* **2020**, *8*, 2014−2018.

(27) Ye, Y.; Zheng, X.; Chen, D.; Deng, Y.; Chen, D.; Hao, Y.; Dai, X.; Jin, Y. Design of the Hole-Injection/Hole-Transport Interfaces for Stable Quantum-Dot Light-Emitting Diodes. *J. Phys. Chem. Lett.* **2020**, *11*, 4649−4654.

(28) Cho, S.-Y.; Oh, N.; Nam, S.; Jiang, Y.; Shim, M. Enhanced device lifetime of double-heterojunction nanorod light-emitting diodes. *Nanoscale* **2017**, *9*, 6103−6110.

(29) Pinner, D. J.; Friend, R. H.; Tessler, N. Transient electroluminescence of polymer light emitting diodes using electrical pulses. *J. Appl. Phys.* **1999**, *86*, 5116−5130.

(30) Pinner, D. J.; Friend, R. H.; Tessler, N. Analysis of the turn-off dynamics in polymer light-emitting diodes. *Appl. Phys. Lett.* **2000**, *76*, 1137−1139.

(31) Park, Y.-S.; Lee, S.; Kim, K.-H.; Kim, S.-Y.; Lee, J.-H.; Kim, J.-J. Exciplex-Forming Co-host for Organic Light-Emitting Diodes with Ultimate Efficiency. *Adv. Funct. Mater.* **2013**, *23*, 4914−4920.

(32) Weichsel, C.; Burtone, L.; Reineke, S.; Hintschich, S. I.; Gather, M. C.; Leo, K.; Lüssem, B. Storage of charge carriers on emitter molecules in organic light-emitting diodes. *Phys. Rev. B* **2012**, *86*, 075204.

(33) Zhang, Z.; Guan, X.; Kang, Z.; Zhang, H.; Zeng, Q.; Yu, R.; Wang, R.; Ji, W. A direct evidence for the energy transfer from phosphorescent molecules to quantum dots in a driving light emitting diode. *Org. Electron.* **2019**, *73*, 337−341.

(34) Kim, H.-M.; Geng, D.; Kim, J.; Hwang, E.; Jang, J. Metal-Oxide Stacked Electron Transport Layer for Highly Efficient Inverted Quantum-Dot Light Emitting Diodes. *ACS Appl. Mater. Interfaces* **2016**, *8*, 28727−28736.

(35) Blauth, C.; Mulvaney, P.; Hirai, T. Transient overshoot and storage of charge carriers on ligands in quantum dot LEDs. *J. Appl. Phys.* **2019**, *126*, 75501.
(36) Wang, T.; Guan, X.; Zhang, H.; Ji, W. Exploring Electronic and Excitonic Processes toward Efficient Deep-Red $CuInS_2$/ZnS Quantum-Dot Light-Emitting Diodes. *ACS Appl. Mater. Interfaces* **2019**, *11*, 36925−36930.
(37) Yuan, Q.; Guan, X.; Xue, X.; Han, D.; Zhong, H.; Zhang, H.; Zhang, H.; Ji, W. Efficient $CuInS_2$/ZnS Quantum Dots Light-Emitting Diodes in Deep Red Region Using PEIE Modified ZnO Electron Transport Layer. *Phys. Status Solidi RRL* **2019**, *13*, 1800575.
(38) Su, Q.; Zhang, H.; Chen, S. Identification of excess charge carriers in InP-based quantum-dot light-emitting diodes. *Appl. Phys. Lett.* **2020**, *117*, 53502.
(39) Wang, Y.; Chen, Z.; Wang, T.; Zhang, H.; Zhang, H.; Wang, R.; Ji, W. Efficient Structure for InP/ZnS-Based Electroluminescence Device by Embedding the Emitters in the Electron-Dominating Interface. *J. Phys. Chem. Lett.* **2020**, *11*, 1835−1839.
(40) Doe, T.; Kitano, K.; Yamamoto, S.; Yamamoto, M.; Goto, K.; Sakakibara, Y.; Kobashi, T.; Yamada, H.; Ueda, M.; Ryowa, T.; Izumi, M.; Arakawa, Y. Evaluation of degradation behavior in quantum dot light-emitting diode with different hole transport materials via transient electroluminescence. *Appl. Phys. Lett.* **2021**, *118*, 203503.
(41) Lee, J.-H.; Lee, S.; Yoo, S.-J.; Kim, K.-H.; Kim, J.-J. Langevin and Trap-Assisted Recombination in Phosphorescent Organic Light Emitting Diodes. *Adv. Funct. Mater.* **2014**, *24*, 4681−4688.
(42) Jung, S.-M.; et al. Modelling charge transport and electro-optical characteristics of quantum dot light-emitting diodes. *npj Comput. Mater.* **2021**, *7*, 122.
(43) Yu, P.; Yuan, Q.; Zhao, J.; Zhang, H.; Ji, W. Electronic and Excitonic Processes in Quantum Dot Light-Emitting Diodes. *J. Phys. Chem. Lett.* **2022**, *13*, 2878−2884.
(44) Nicolai, H. T.; Hof, A.; Oosthoek, J. L. M.; Blom, P. W. M. Charge Transport and Recombination in Polyspirobifluorene Blue Light-Emitting Diodes. *Adv. Funct. Mater.* **2011**, *21*, 1505−1510.
(45) Karg, S.; Dyakonov, V.; Meier, M.; Riess, W.; Paasch, G. Transient electroluminescence in poly(p-phenylenevinylene) light-emitting diodes. *Synth. Met.* **1994**, *67*, 165−168.
(46) Ranke, P.; Bleyl, I.; Simmerer, J.; Haarer, D.; Bacher, A.; Schmidt, H. W. Electroluminescence and electron transport in a perylene dye. *Appl. Phys. Lett.* **1997**, *71*, 1332−1334.
(47) Blom, P. W. M.; Vissenberg, M. C. J. M. Dispersive Hole Transport in Poly({*p*}-Phenylene Vinylene). *Phys. Rev. Lett.* **1998**, *80*, 3819−3822.
(48) Qian, L.; Zheng, Y.; Xue, J.; Holloway, P. H. Stable and efficient quantum-dot light-emitting diodes based on solution-processed multilayer structures. *Nat. Photonics* **2011**, *5*, 543−548.
(49) Redecker, M.; Bradley, D. D.; Inbasekaran, M.; Wu, W. W.; Woo, E. P. High Mobility Hole Transport Fluorene-Triarylamine Copolymers. *Adv. Mater.* **1999**, *11*, 241−246.
(50) Ginger, D. S.; Greenham, N. C. Charge injection and transport in films of CdSe nanocrystals. *J. Appl. Phys.* **2000**, *87*, 1361−1368.
(51) Yu, D.; Wehrenberg, B. L.; Jha, P.; Ma, J.; Guyot-Sionnest, P. Electronic transport of n-type CdSe quantum dot films: Effect of film treatment. *J. Appl. Phys.* **2006**, *99*, 104315.
(52) Nam, S.; Oh, N.; Zhai, Y.; Shim, M. High efficiency and optical anisotropy in double-heterojunction nanorod light-emitting diodes. *ACS Nano* **2015**, *9*, 878−85.
(53) Hagfeldt, A.; Graetzel, M. Light-Induced Redox Reactions in Nanocrystalline Systems. *Chem. Rev.* **1995**, *95*, 49−68.
(54) Stouwdam, J. W.; Janssen, R. A. J. Red, green, and blue quantum dot LEDs with solution processable ZnO nanocrystal electron injection layers. *J. Mater. Chem.* **2008**, *18*, 1889−1894.
(55) Porter, V. J.; Geyer, S.; Halpert, J. E.; Kastner, M. A.; Bawendi, M. G. Photoconduction in Annealed and Chemically Treated CdSe/ZnS Inorganic Nanocrystal Films. *J. Phys. Chem. C* **2008**, *112*, 2308−2316.
(56) Yu, D.; Wang, C.; Guyot-Sionnest, P. n-Type Conducting CdSe Nanocrystal Solids. *Science* **2003**, *300*, 1277−1280.
(57) Straus, D. B.; Goodwin, E. D.; Gaulding, E. A.; Muramoto, S.; Murray, C. B.; Kagan, C. R. Increased Carrier Mobility and Lifetime in CdSe Quantum Dot Thin Films through Surface Trap Passivation and Doping. *J. Phys. Chem. Lett.* **2015**, *6*, 4605−4609.
(58) Zhang, H.; Yuan, Q.; Wang, T.; Xue, X.; Yuan, Y.; Zhang, H.; Zhou, M.; Ji, W. Unraveling the effect of shell thickness on charge injection in blue quantum-dot light-emitting diodes. *Appl. Phys. Lett.* **2021**, *119*, 243504.
(59) Blauth, C.; Mulvaney, P.; Hirai, T. Transient overshoot and storage of charge carriers on ligands in quantum dot LEDs. *J. Appl. Phys.* **2019**, *126*, 075501.
(60) Barth, S.; Müller, P.; Riel, H.; Seidler, P. F.; Riess, W.; Vestweber, H.; Bässler, H. Electron mobility in tris(8-hydroxy-quinoline)aluminum thin films determined via transient electro-luminescence from single- and multilayer organic light-emitting diodes. *J. Appl. Phys.* **2001**, *89*, 3711−3719.
(61) Reineke, S.; Lindner, F.; Huang, Q.; Schwartz, G.; Walzer, K.; Leo, K. Measuring carrier mobility in conventional multilayer organic light emitting devices by delayed exciton generation. *Phys. Status Solidi B* **2008**, *245*, 804−809.
(62) Liu, R.; Gan, Z.; Shinar, R.; Shinar, J. Transient electro-luminescence spikes in small molecular organic light-emitting diodes. *Phys. Rev. B* **2011**, *83*, 245302.
(63) Pu, C.; Dai, X.; Shu, Y.; Zhu, M.; Deng, Y.; Jin, Y.; Peng, X. Electrochemically-stable ligands bridge the photoluminescence-electroluminescence gap of quantum dots. *Nat. Commun.* **2020**, *11*, 937.
(64) Kwak, J.; Bae, W. K.; Lee, D.; Park, I.; Lim, J.; Park, M.; Cho, H.; Woo, H.; Yoon, D. Y.; Char, K.; Lee, S.; Lee, C. Bright and Efficient Full-Color Colloidal Quantum Dot Light-Emitting Diodes Using an Inverted Device Structure. *Nano Lett.* **2012**, *12*, 2362−2366.
(65) Dai, X.; Zhang, Z.; Jin, Y.; Niu, Y.; Cao, H.; Liang, X.; Chen, L.; Wang, J.; Peng, X. Solution-processed, high-performance light-emitting diodes based on quantum dots. *Nature* **2014**, *515*, 96−99.

https://doi.org/10.1021/acs.nanolett.2c03564
Nano Lett. 2022, 22, 9500−9506